Polarization-engineered removal of buffer leakage for GaN transistors

Yu Cao,[a] Tom Zimmermann, Huili Xing, and Debdeep Jena
Department of Electrical Engineering, University of Notre Dame, Indiana 46556, USA

A dopant-free epitaxial technique is developed to achieve highly insulating buffers on semi-insulating GaN templates for nitride high electron mobility transistors by using the large polarization fields. The buffer leakage current density is reduced by several orders of magnitude, exhibiting outstanding insulating and breakdown properties. The simple polarization- and heterostructure-based solution should prove highly attractive for GaN high electron mobility transistors for analog (rf), digital, and high-voltage switching applications. © *2010 American Institute of Physics*. [doi:10.1063/1.3293454]

III-V nitride semiconductor based high electron mobility transistors (HEMTs) have been extensively developed recently for high speed/high power device applications.[1–4] The structure of nitride HEMTs usually consists of an AlGaN (AlN, or AlInN) barrier and a GaN buffer layer. The polarization-induced two-dimensional electron gas (2DEG) formed at the AlGaN(AlN)/GaN heterojunction serves as the transistor channel. Due to the lack of native GaN substrates, SiC, sapphire, semi-insulating (SI) GaN templates on sapphire, and high-resistivity silicon are the most widely used as starting substrates for HEMT epitaxy. SiC (owing to high thermal conductivity) and native GaN lattice matched substrates are ideal for HEMT growths. GaN templates on sapphire are the closest to native GaN substrates and are cost-effective, though the low thermal conductivity of sapphire limits very high power rf applications.

In the epitaxial growth on both SiC and GaN templates, shallow dopant impurities such as silicon and oxygen exist at the regrowth interface of SiC/GaN or SI GaN/GaN. A conducting path is formed at the regrowth interface due to the impurities, and causes leakage.[5–8] This adversely affects both analog and digital device applications of HEMTs. In digital applications, the on/off ratio is much degraded, and for high-frequency applications, the device speed decreases. For high-voltage applications, buffer leakage severely degrades the breakdown property of nitride HEMTs.

Various solutions to the problem of buffer leakage have been attempted such as (a) deep level dopants[9–11] and (b) thick AlN nucleation grown in N-rich regime followed by a two-step buffer on SiC substrates.[6,7,12] Since the critical thickness of AlN on GaN is less than 7 nm,[13] these techniques do not transfer to SI GaN templates. In this letter, we present a dopant-free thin-layer solution by exploiting the giant polarization fields in III-V nitride heterostructures.

Commercially available Ga-face GaN templates consisting of ~ 2 μm Fe-doped SI GaN layers on sapphire[14] were used for epitaxy. To highlight the problem of buffer leakage, an AlN/GaN HEMT structure was first grown by molecular beam epitaxy (MBE). At the regrowth interface, ~ 2 monolayers of Ga were deposited at a thermocouple temperature of $T_{TC} \sim 600$ °C (the substrate temperature is ~ 60 °C higher) in ~ 10 s before opening the nitrogen supply. This ensures a metal-rich nucleation regime. Thereafter, T_{TC} was

increased to 660 °C and a ~ 234 nm thick unintentional doped (UID) GaN layer, followed by a $t_{AlN} \sim 3$ nm AlN cap layer was grown. The metal and nitrogen fluxes and pressures used have been reported earlier.[15] A polarization-induced 2DEG formed at the AlN/GaN heterojunction. Hall-effect measurement with indium contacts yielded a mobility of $\mu = (1646, 6740)$ cm^2/V s at [room temperature (RT), and 77 K], respectively. The 2DEG charge density was $n_s \sim (2.0, 1.9) \times 10^{13}$ cm^{-2} at (RT, 77 K), respectively. The charge difference between RT and 77 K is $\sim 10^{12}$ cm^{-2}, consistent with earlier reports,[13,15] and indicative of freezeout of shallow dopants in a parallel conduction path.

To test the buffer leakage in this control sample, 100×100 μm^2 pads of Ti/Al/Ni/Au Ohmic metal stack were deposited with a separation of ~ 6 μm and annealed to form Ohmic contacts with the 2DEG. Reactive-ion etching was then performed using the pads as masks. A etch depth of ~ 75 nm was verified by atomic force microscope (AFM) scans. This etch process removes the 2DEG conducting channel, and any current between the contacts must flow through unintentional leakage paths [see Fig. 1(a)]. The measured leakage current density is plotted in Fig. 1(a). The
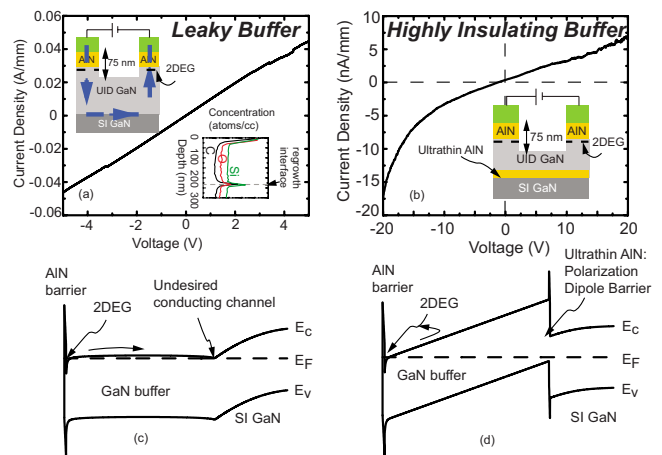

FIG. 1. (Color online) (a) Leakage current density in the buffer vs applied voltage for the control sample. Inset shows the SIMS atomic concentrations against the depth with strong impurity peaks of silicon, oxygen and carbon at the regrowth interface. (b) Very low buffer leakage in the nA/mm range using an ultrathin AlN NL. [(c) and (d)] Energy band diagrams of the two structures showing removal of parallel conduction path and an electron back-barrier.
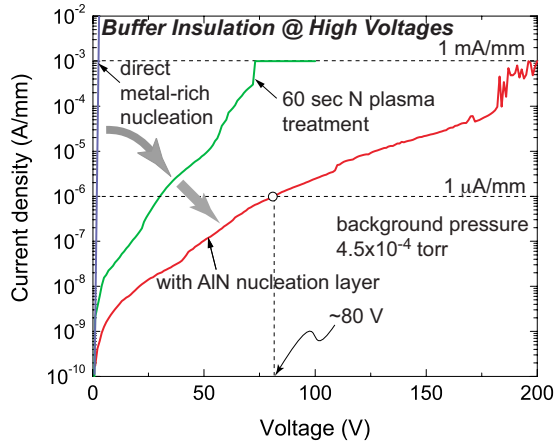
a)Electronic mail: ycao1@nd.edu.

FIG. 2. (Color online) Comparison of buffer leakage in the control sample, with 60 s N_2 plasma treatment, and with 1.5 nm AlN NL.
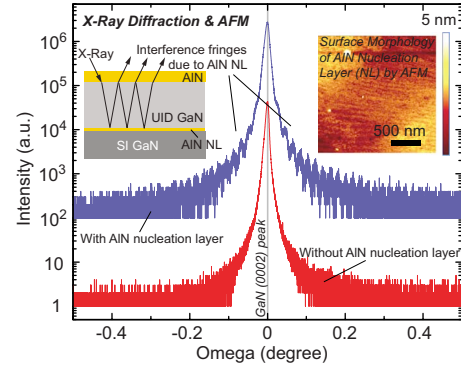

FIG. 3. (Color online) X-ray measurement results, showing cavity resonance fringes caused by the AlN NL, and its absence in the control sample. The inset shows a 2×2 μm^2 AFM scan with the smooth surface of the AlN NL.

current density reaches more than 40 mA/mm at ± 5 V bias, which is just $25\times$ smaller than the current that flows through the 2DEG channel (~ 1000 mA/mm) in the on state of a typical nitride HEMT. The inset in Fig. 1(a) shows a secondary ion mass spectrometry (SIMS) scan of unintentional impurities. Large peak concentrations of silicon ($\sim 10^{19}/cm^3$), oxygen ($\sim 10^{18}/cm^3$), and carbon ($\sim 10^{18}/cm^3$) were found at the regrowth interface. Both oxygen and silicon are n-type dopants in GaN. As shown in the energy band diagram[16] in Fig. 1(c), the potential barrier between the electrons in the 2DEG and the unintentional highly doped regrowth interface is easily surmountable, especially at high voltages, and this interface leads to high leakage current.

In comparison, the drastic effect of an ultrathin AlN nucleation layer (NL) at the regrowth interface is shown in Fig. 1(b). The buffer leakage current density is cut down by a factor of 10^7 at 4 V, and to less than 20 nA/mm at 20 V—this is the major result of this work. The AlN layer introduces a polarization-induced charge dipole that bends the bands as shown in the energy band diagram in Fig. 1(d)—it removes the conductive layer by pulling up the conduction band edge, and in the process introduces a desirable "back-barrier" to prevent electrons in the 2DEG from being injected deep into the substrate. The rest of this letter describes how this solution was developed, and its impact on AlN/GaN HEMTs.

The first attempted solution to eliminate the leakage path at the regrown interface comprised of N_2 plasma treatment of the regrowth interface. The surface of the GaN template was exposed to a $P_{N_2} = 400$ W rf nitrogen plasma at $T_{TC} \sim 660$ °C in the MBE growth chamber for 60 s prior to growth with metal-rich nucleation. The rest of the growth proceeded as that for the control sample. This sample yielded $\mu = (1542, 4979)$ cm^2/V s at (RT, 77 K), respectively, with a 2DEG charge density $n_s \sim (2.27, 2.24) \times 10^{13}$ cm^{-2} at (RT, 77 K), the smaller freezeout indicative of a smaller density of active shallow dopants. To prevent breakdown through air, high-voltage measurements were performed at RT in a vacuum chamber at a pressure of $\sim 4.5 \times 10^{-4}$ Torr. As shown in Fig. 2, the nitrogen plasma treated sample exhibited a leakage current density $\sim 10^{-8}$ A/mm at 4 V, more than six orders of magnitude lower than the control sample. Partial formation of SiN is a likely reason for the reduction in buffer leakage and lower freezeout. However, the leakage

current increased rapidly at higher voltages, reaching 1 $\mu A/mm$ at ~ 30 V, and 1 mA/mm at ~ 70 V. These voltages are far below the potential of the GaN material system, and from Fig. 1(c), the ease of carriers in the 2DEG leaking into the regrowth interface can be effectively cut off by the incorporation of heterostructure design.

Motivated by the energy band diagram in Fig. 1(d), an ultrathin (~ 1.5 nm) AlN NL was grown on SI GaN. The growth was performed at $T_{TC} \sim 660$ °C, $P_{N_2} = 400$ W for the 1.5 nm AlN NL and $P_{N_2} = 275$ W for the rest of the GaN/AlN heterostructure. This instant switching from a high to low plasma power ensured a nitrogen-rich AlN NL followed by a metal rich GaN/AlN growth. X-ray diffraction measurement (Fig. 3) showed cavity resonance fringes due to the existence of the thin AlN NL, which were absent in control samples. The surface morphology of the NL was studied by AFM on a sample with just the AlN NL-the inset of Fig. 3 shows a smooth surface with a root-mean-square roughness of ~ 0.57 nm over a 2×2 μm^2 scan. This sample yielded $\mu = (1516, 5242)$ cm^2/V s at (RT, 77 K) respectively, with a 2DEG charge density $n_s \sim (2.08, 2.11) \times 10^{13}$ cm^{-2} at (RT, 77 K). The low-temperature 2DEG density is actually *higher*, hinting at the complete removal of parallel conduction due to shallow dopants. The small increase in the 2DEG density at low temperature could be related to the relative change in band gaps of GaN and AlN, but needs further investigation to be definitive.

As shown in Fig. 2, the leakage current density in this sample reached 1 $\mu A/mm$ at the bias of ~ 80 V and 1 mA/mm at ~ 200 V. Compared to the control sample, the buffer leakage in this structure with a 1.5 nm AlN nucleation is about seven orders lower in the magnitude. The ultrathin epitaxial nitrogen-rich AlN buffer thus leads to outstanding insulating and breakdown properties. Capacitance-voltage profiling (not shown) indicated the existence of a leakage path at the regrowth interface in the control sample, and a complete removal of this channel in the structure with the AlN NL. We note here that in order to obtain the highly insulating buffer, it is essential to employ a nitrogen-rich AlN NL; a metal-rich AlN layer leads to substantial leakage, quite possibly since the excess metal allows the diffusion of oxygen and silicon dopant atoms from the regrowth interface into the buffer layer.[17]

The reduced buffer leakage using the epitaxial AlN NL had a substantial effect on the off-state performance of
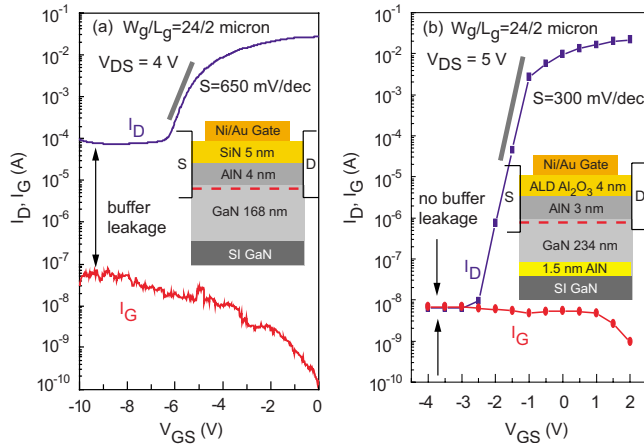
FIG. 4. (Color online) The transfer characteristics show that (a) the control sample suffers from severe buffer leakage, and (b) in the sample with the AlN NL the buffer leakage has been decreased lower than the gate leakage.

AlN/GaN HEMTs. Both the HEMTs with and without the AlN NL exhibit gate modulation of the drain current, but the impact of the AlN NL is more clearly seen by comparing the logarithmic I_D, I_G versus V_{GS} transfer characteristics in Figs. 4(a) and 4(b). The gate width/length (W_g/L_g) of both the HEMTs are $24/2$ μm. The control HEMT sample shows a substantial difference between the drain and gate currents, a clear signature of leakage current flowing through the regrowth interface. This leakage sets a floor of relatively high off-state current, a feature that is highly undesirable. The HEMT with the AlN NL solves this problem; the drain and gate currents become equal below -2.5 V gate bias. In the process of buffer leakage removal, the on/off ratio improves from $\sim 10^2$ to 10^6, a feature that is highly attractive for both analog and digital applications. In addition, the natural back-barrier introduced due to the band offsets and polarization dipole as shown in the energy band diagram in Fig. 1(b) can potentially enable reduced short-channel effects for shorter gate length HEMTs. The combination of lower buffer leakage and the back barrier leads to a much steeper subthreshold slope (300 mV/dec with the AlN NL compared to 650 mV/dec without it).

In conclusion, a polarization-based highly insulating buffer has been developed on SI GaN templates for GaN HEMTs by RF plasma source MBE. An ultrathin epitaxial AlN NL solves the buffer leakage problem, and is a highly attractive alternative to competing methods since (a) it is a dopant-free approach, (b) it saves source materials, (c) growth time and other resources incurred in the epitaxy process. It will become increasingly important for nitride HEMTs for analog (rf) and digital (power switching) applications, especially as native GaN substrates become more widely available in the near future.

[1] N. G. Weimann, M. J. Manfra, and R. Wachtler, IEEE Electron Device Lett. **24**, 57 (2003).
[2] S. Rajan, P. Waltereit, C. Poblenz, S. J. Heikman, D. S. Green, J. S. Speck, and U. K. Mishra, IEEE Electron Device Lett. **25**, 247 (2004).
[3] R. M. Chu, L. K. Shen, N. Fichtenbaum, D. Brown, Z. Chen, S. Keller, S. P. DenBaars, and U. K. Mishra, IEEE Electron Device Lett. **29**, 974 (2008).
[4] Y. Pei, C. Poblenz, A. L. Corricon, R. M. Chu, L. K. Shen, J. Speck, and U. K. Mishra, Electron Lett. **44**, 598 (2008).
[5] J. P. Ao, T. Wang, D. Kikuta, Y. H. Liu, S. Sakai, and Y. Ohno, Jpn. J. Appl. Phys., Part 1 **42**, 1588 (2003).
[6] D. F. Storm, D. S. Katzer, S. C. Binari, B. V. Shanabrook, L. Zhou, and D. J. Smith, Appl. Phys. Lett. **85**, 3786 (2004).
[7] C. Poblenz, P. Waltereit, S. Rajan, U. K. Mishra, J. S. Speck, P. Chin, I. Smorchkova, and B. Heying, J. Vac. Sci. Technol. B **23**, 1562 (2005).
[8] L. Zhou, D. J. Smith, D. F. Storm, D. S. Katzer, S. C. Binari, and B. V. Shanabrook, Appl. Phys. Lett. **88**, 011916 (2006).
[9] H. Tang, J. B. Webb, J. A. Bardwell, S. Raymond, J. Salzman, and C. Uzan-Saguy, Appl. Phys. Lett. **78**, 757 (2001).
[10] D. F. Storm, D. S. Katzer, S. C. Binari, E. R. Glaser, B. V. Shanabrook, and J. A. Roussos, Appl. Phys. Lett. **81**, 3819 (2002).
[11] P. B. Klein, S. C. Binari, K. Ikossi, A. E. Wickenden, D. D. Koleske, and R. L. Henry, Appl. Phys. Lett. **79**, 3527 (2001).
[12] P. Waltereit, C. Poblenz, S. Rajan, F. Wu, U. K. Mishra, and J. S. Speck, Jpn. J. Appl. Phys., Part 2 **43**, L1520 (2004).
[13] Y. Cao and D. Jena, Appl. Phys. Lett. **90**, 182112 (2007).
[14] Templates were obtained from LumiLog, http://www.lumilog.com.
[15] Y. Cao, K. Wang, A. Orlov, H. Xing, and D. Jena, Appl. Phys. Lett. **92**, 152112 (2008).
[16] The energy band diagrams were calculated using a self-consistent solution of Poisson and Schrodinger equations with the software program 1DPoisson, freely downloadable from http://www.nd.edu/~gsnider.
[17] W. E. Hoke, A. Torabi, J. J. Mosca, and T. D. Kennedy, J. Vac. Sci. Technol. B **25**, 978 (2007).